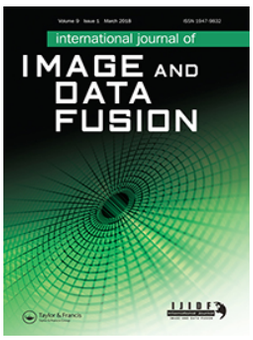

International Journal of Image and Data Fusion

ISSN: 1947-9832 (Print) 1947-9824 (Online) Journal homepage: http://www.tandfonline.com/loi/tidf20

A novel image fusion algorithm using an NSCT and a PCNN with digital filtering

Guoan Yang, Chihiro Ikuta, Songjun Zhang, Yoko Uwate, Yoshifumi Nishio & Zhengzhi Lu

To cite this article: Guoan Yang, Chihiro Ikuta, Songjun Zhang, Yoko Uwate, Yoshifumi Nishio & Zhengzhi Lu (2018) A novel image fusion algorithm using an NSCT and a PCNN with digital filtering, International Journal of Image and Data Fusion, 9:1, 82-94, DOI: 10.1080/19479832.2017.1384763

To link to this article: https://doi.org/10.1080/19479832.2017.1384763

INTERNATIONAL JOURNAL OF IMAGE AND DATA FUSION, 2018
VOL. 9, NO. 1, 82–94
https://doi.org/10.1080/19479832.2017.1384763

Taylor & Francis
Taylor & Francis Group

LETTER

A novel image fusion algorithm using an NSCT and a PCNN with digital filtering

Guoan Yang[a], Chihiro Ikuta[b], Songjun Zhang[c], Yoko Uwate[b], Yoshifumi Nishio[b] and Zhengzhi Lu[a]

[a]School of Electronic and Information Engineering, Xi'an Jiaotong University, Shaanxi, China; [b]Department of Electrical and Electronics Engineering, Tokushima University, Tokushima, Japan; [c]School of Mathematics and Statistics, Xi'an Jiaotong University, Shaanxi, China

ABSTRACT

Image fusion is an important task in both image processing and computer vision research that use multisensor processing and multiscale analysis. This paper proposed a novel image fusion algorithm using a nonsubsampled contourlet transform (NSCT) and a pulse-coupled neural network (PCNN) with digital filtering. First, we decomposed two original images into a low-frequency and a series of high-frequency subband coefficients based on the NSCT and repeated that step for the next low-frequency subband. Second, each low-frequency subband coefficient in different levels in the frequency domain for both images was duplicated, and then these low-frequency subband coefficients of different levels from two different images were processed through a Laplacian filter and an average filter. The Laplacian filter can improve the performance of both edge and texture representation; the average filter can implement image smoothing for creating a superior reconstruction of an image via the low-frequency subband coefficients of the frequency domain in image processing. Moreover, the coupling coefficients from different images were fused by using the PCNN. Finally, reconstructed a fused image based on low- and high-frequency subband coefficients in different scales and directions using the inverse NSCT. Experimental results show that the proposed algorithm is superior to state-of-the-art conventional image fusion algorithms.

ARTICLE HISTORY
Received 3 February 2017
Accepted 13 September 2017

KEYWORDS
Average filter; image fusion; Laplacian filter; nonsubsampled contourlet transform; pulse-coupled neural network

1. Introduction

For many kinds of images, such as visible images, multifocus images, multisensor images, synthetic aperture radar (SAR) images and infrared images, image fusion processing can make their respective advantages mutually complementary. Therefore, the image fusion algorithm is an important part of both image processing and computer vision research (Zheng *et al*. 2007, Yang and Li 2010, Wang *et al*. 2013a). In recent years, several new image fusion algorithms have been reported and widely applied in image processing, computer vision, pattern recognition and so on (Qu *et al*. 2008, Li and Yang 2010, Jang *et al*. 2012).

CONTACT Guoan Yang gayang@mail.xjtu.edu.cn School of Electronic and Information Engineering, Xi'an Jiaotong University, Shaanxi 710049, China

For an image fusion algorithm, it is crucial to select important pixels in the spatial domain from each image via corresponding subband coefficients of the frequency domain (Chan *et al*. 2013, Stokman and Gevers 2007). However, because an original image of nature contains much important and complex information in the spatial domain, detecting and fusing those pixels for various images is difficult. We know that the contourlet transform is a new two-dimensional extension of the wavelet transform that uses multiscale and directional filter banks (Núñez *et al*. 1999, Petrovic and Xydeas 2004, Yang *et al*. 2010). A contourlet transform decomposes the original image into some coefficients in low- and high-frequency subbands in every level of the image. This scheme then provides sparsity to the solutions of multiscale decompositions (Yang *et al*. 2008). Therefore, each sparse coefficient with broad energy can easily be processed because it contains only the important information. For a developed algorithm, a nonsubsampled contourlet transform (NSCT) has been proposed by Da Cunha *et al*. (2006). The NSCT has a more thorough shift-invariant property than the contourlet transform, which leads to better frequency selectivity, directivity and regularity (Zhou *et al*. 2005, Xie *et al*. 2010, Wang *et al*. 2013b). In the field of artificial neural networks, a pulse-coupled neural network (PCNN) has been proposed by Eckhorn *et al*. (1990). The method was developed based on experimental observations of synchronous pulse bursts in a cat visual cortex (Johnson and Padgett 1999). Therefore, a PCNN can be characterised by the global coupling and pulse synchronisation of neurons and has excellent performance in image edge-detection applications (Wang *et al*. 2010, 2016). Although image fusion research has been carried out for 30 years, research results based on a hybrid NSCT and PCNN algorithm are very few and insufficient. However, recently several image fusion algorithms based on NSCT and PCNN have been developed, for example, a spatial frequency-motivated PCNN in an NSCT domain (Qu *et al*. 2008), a stationary wavelet-based NSCT–PCNN (Yang *et al*. 2009), an NSCT–PCNN for visible and infrared images (Ge and Li 2010) and a simplified PCNN in an NSCT domain (Fu *et al*. 2012). Those image fusion methods have resulted in improved fusion performance for various image applications.

In this paper, we first use an NSCT for implementing multiscale and multidirectional decomposition, and a PCNN to achieve image fusion. Furthermore, we propose a novel image fusion approach based on the hybrid NSCT–PCNN with digital filtering that uses two different filters: a Laplacian filter and an average filter. Because coefficient fusion was implemented before image fusion using the PCNN, we further found that the quality of a fusion image is improved by using a PCNN with digital filtering in an NSCT domain, resulting in a better image fusion performance than that with other hybrid NSCT and PCNN algorithms.

This paper is organised as follows: In Section 2, we describe an image fusion algorithm using a hybrid NSCT and PCNN method. In Section 3, we propose a new image fusion algorithm using a hybrid NSCT and a PCNN with digital filtering. In Section 4, we show the experimental results and compare them with those of the state of the art methods using the hybrid NSCT and PCNN. Finally, in Section 5, we discuss the conclusions.

2. Image fusion algorithm using the hybrid NSCT and PCNN

An image fusion algorithm using the hybrid NSCT and PCNN has three main steps of multiresolution analysis. In the first step, two original images are decomposed into some

frequency subband coefficients of different directions in every scale by using an NSCT. In the second step, every pair of coefficients generated by the different original images is compared and fused by a PCNN. Finally, the fused coefficients are reconstructed into one new image by an inverse NSCT.

In the NSCT (Zhou *et al*. 2005, Zhang and Guo 2009), up-sampling and down-sampling do not exist, so a PCNN can easily be used to fuse the coefficients mentioned above. In addition, the NSCT uses two different filter banks: a pyramid filter bank to implement a multiscale decomposition and a directional filter bank to implement directional decomposition, as shown in Figure 1 (Da Cunha *et al*. 2006). For the multi-scale decomposition, an image is decomposed into low- and high-frequency subband coefficients, and those operations are repeated at different scales. Then, the coefficients are decomposed into a low-frequency component and some directional components in the high-frequency banks in different scales. Image processing accuracy can accordingly be improved by decomposing an image into large frequency levels and direction numbers, although the computational cost becomes greater. Generally, for image multi-scale decomposition, in the different scales where an image can be decomposed into different numbers of directions subband, an image can be decomposed at each scale into any arbitrary power-of-twos number of directions subbands.

A PCNN was proposed by Thomas Lindblad for the application of that mechanism in 1998 (Lindblad and Kinser 2005). It is known that this method can be applied to image understanding and can also be applied to image fusion (Johnson and Padgett 1999, Wang *et al*. 2010). The neurons in a PCNN have a high response to image edges, so it can be effectively adapted to edge detection, feature extraction, image retrieval and so on. Image edges are important for image processing and computer vision because they contain

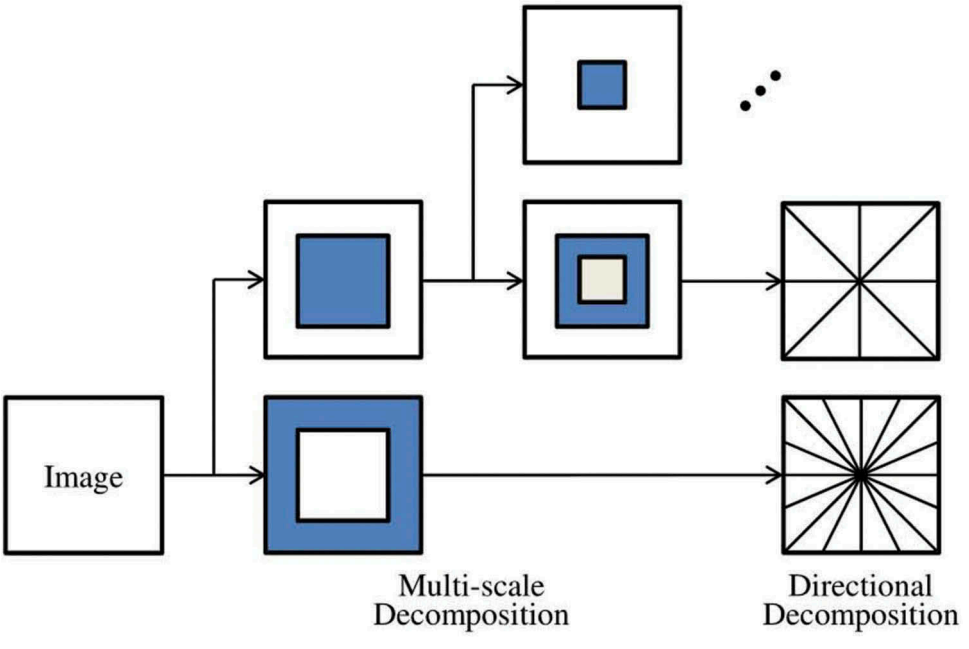

Figure 1. An NSCT for image decomposition.

important information and most of the energy of the image. Also, there are already very sparse subband coefficients of different scales after an NSCT operation, so when a PCNN is used in image processing, corresponding to a sparse coefficient, one pixel datum in an image can match up with one neuron. In addition, all the coefficients in the NSCT domain are done sparsely, so the use of the actual neuron number is significantly reduced. Generally, a PCNN has two main components; a feeding part and a linking part (Figure 2).

The feeding part is described by

$$F_{ij}^{\ell,k}(n) = S_{ij}^{\ell,k}, \tag{1}$$

where F is an output of the feeding part and S is an external stimulus.

The linking part is expressed by the following equation:

$$L_{ij}^{\ell,k}(n) = e^{-\alpha_L} L_{ij}^{\ell,k}(n-1) + V_L \sum\nolimits_{pq} W_{ij,pq} Y_{ij,pq}(n-1)\,, \tag{2}$$

where L is an output of the linking part, V is a normalisation coefficient and W is the weights of connections with other neurons.

An internal state is calculated by outputs of the feeding and linking parts, as shown in

$$U_{ij}^{\ell,k}(n) = F_{ij}^{\ell,k}(n) \times \left[1 + \beta L_{ij}^{\ell,k}(n)\right], \tag{3}$$

where U represents an internal state. The output of the neuron is calculated depending on the comparison between the internal state and a threshold, and the threshold is expressed as

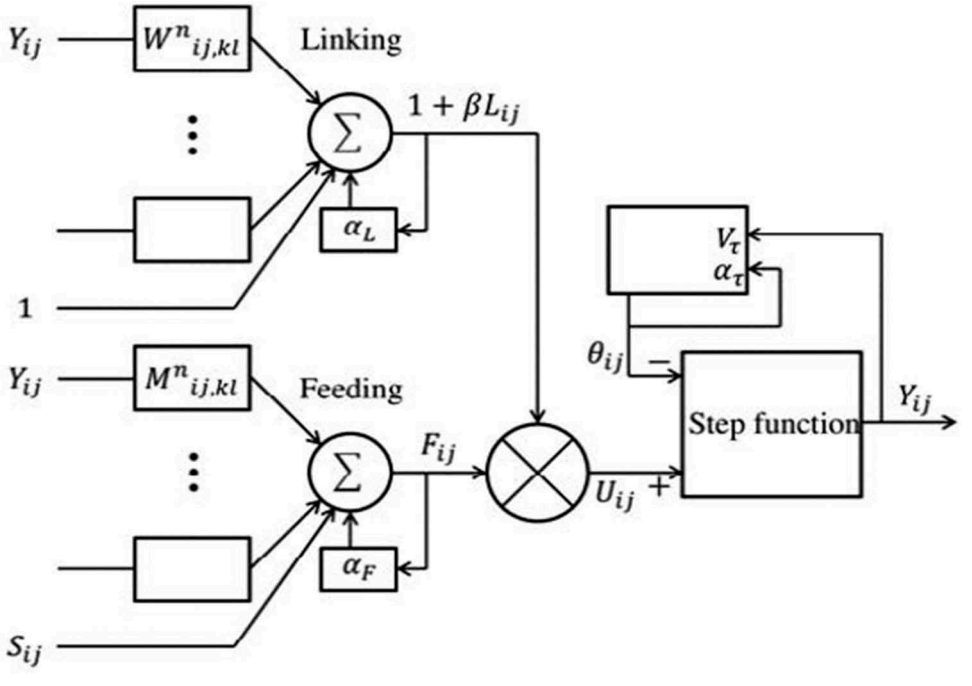

Figure 2. Block diagram of a single neuron of the PCNN.

$$\theta_{ij}^{\ell,k}(n) = e^{-\alpha_\theta}\theta_{ij}^{\ell,k}(n-1) + V_\theta Y_{ij}(n-1), \tag{4}$$

where θ is a threshold of the PCNN and where a step function is defined as an activation function. Here, the output of the neuron is indicated by

$$Y_{ij}(n) = \begin{cases} 1, & U_{ij}^{\ell,k}(n) > \theta_{ij}^{\ell,k}(n) \\ 0, & \text{otherwise} \end{cases}. \tag{5}$$

Hence, we investigated the parameters and performance of the PCNN model (Figure 2) and finally chose those parameters by using a heuristic method whose performance of the PCNN model was excellent.

In the simulation, we input the decomposition coefficients of two images to the PCNN, whereas in an image fusion application, each neuron receives and processes only 1 pixel with the corresponding coefficient in the frequency domain. Therefore, the number of neurons depends on the image size and the sparse coefficients. The PCNN iteratively processes and fuses two types of coefficients in the frequency domain as the same number for various images. After that, the two images processed by the PCNN are analysed and fused by

$$I_{ij}^{\ell,k} = \begin{cases} A_{ij}^{\ell,k}, & Y_{ij}^{A} > Y_{ij}^{B} \\ B_{ij}^{\ell,k}, & \text{otherwise} \end{cases}, \tag{6}$$

where I is a fused coefficient, A is the coefficients of the image A and B is the coefficients of the image B.

3. Proposed image fusion algorithm

In this paper, we propose a novel low-frequency coefficients processing approach in the first two levels for image fusion. Usually, the high-frequency region in the spatial domain for an image possesses the edge and texture information, which makes the grey value greater than the low-frequency region of some flat areas in an image. We found that most of the energy of a natural image is concentrated in the high-frequency region in the spatial domain, and these coefficients possess some greater grey values in the spatial domain, where they belong to the low-frequency region in the frequency domain. Therefore, we derived a novel idea that the quality of an image in the spatial domain might be improved by adjusting the low-frequency subband coefficients of the image in the frequency domain. The process flowchart of the proposed image fusion algorithm is shown in Figure 3.

In the proposed algorithm, two original images were decomposed into a low-frequency and several high-frequency subband coefficients in the different scales by using the NSCT. Among them, five levels of image decomposition were obtained by using a pyramidal filter, and we implemented every level number of directional subbands to be the second-power numbers of the levels passing through the directional filter banks in the NSCT. In addition, one low-frequency subband can be obtained, and 62 high-frequency subband can be obtained in whole levels. The proposed algorithm adopted mainly a digital filtering technique to process the subband coefficients in the frequency domain. Among them, the subband coefficients of the first two lower levels from NSCT

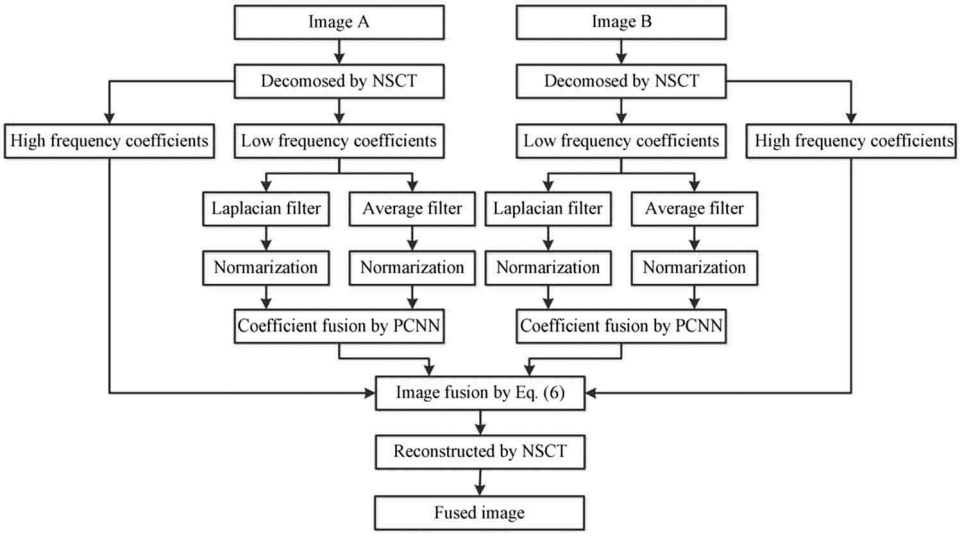

Figure 3. Process of the proposed image fusion algorithm.

decomposition were duplicated and then processed by using a Laplacian filter and an average filter, respectively, and the corresponding subband coefficients were generated. Moreover, we could implement the coefficients fusion of an image using the PCNN after normalising the two kinds of coefficients from the Laplacian and average filters. Finally, a fusion processing of different images was passed through Equation (6).

The Laplacian filter is an edge-detection operator; however, we found that it can also enable some low-frequency regions to become high-frequency regions in the spatial domain for an image by adjusting some low-frequency coefficients in the frequency domain, thus enhancing the edge effects and the edge information of an image. Therefore, some greater coefficients are preserved when most of the smaller coefficients in the frequency domain are cleared by using a threshold of the NSCT. In summary, the Laplacian filter can enhance borders and edges for difference contrasts, and the average filter can smooth the local information of an image. Moreover, to eliminate effects of different transformations, the low-frequency coefficients will be normalised after Laplacian and average filtering.

On the contrary, all coefficients of different bands in five levels are thereby generated for reconstructing the original image using an inverse NSCT. In addition, the matrix of the Laplacian filter is described by the following equation:

$$\text{Laplacian filter} = \begin{bmatrix} -1 & -1 & -1 \\ -1 & 9 & -1 \\ -1 & -1 & -1 \end{bmatrix}. \tag{7}$$

On the other hand, here the average filter is expressed by the following equation:

$$\text{Average filter} = \begin{bmatrix} 0.11 & 0.11 & 0.11 \\ 0.11 & 0.12 & 0.11 \\ 0.11 & 0.11 & 0.11 \end{bmatrix}. \tag{8}$$

Therefore, the two types of coefficients from the two different filters above are fused by using the PCNN image fusion algorithm. Based on PCNN iterative processing, we can here obtain the neuron output value by using pixel values of both the fused coefficients, which are generated from the two different filters above. Another image was processed using the same algorithm procedure. Finally, we can fuse both coefficients from two images and the high-frequency subband coefficients coming from the NSCT decomposition by using Equation (6). In addition, we can reconstruct the fused image using all the low- and high-frequency coefficients in the different levels of direction subbands by an inverse NSCT. Here, we found that the quality of a fused image was improved by filtering the low-frequency coefficients in the NSCT domain, because the Laplacian filter and the average filter increased the intensity of the image in the high-frequency region of spatial domain, and these coefficients were effectively preserved when all smaller coefficients in the frequency domain were removed using an NSCT threshold.

4. Performance evaluations

In this section, we compare the image fusion performance of a state-of-art conventional algorithm with that of the proposed algorithm. The state-of-art conventional algorithm was the NSCT–PCNN-based image fusion algorithm. Our algorithm decomposed the image into the coefficients of the low- and high-frequency subbands in various levels by using the NSCT, which can generate sparse coefficients at various-direction subbands in each level for an image, and then chose each pixel with the corresponding coefficients based on the response of the PCNN. In the experiments, we prepared three kinds of original images: multifocus images, multisensor images and SAR images, as shown in Figure 4 (including a1 and a2, b1 and b2, c1 and c2, d1 and d2, e1 and e2, and f1 and f2). For an evaluation of the image fusion performance, we used mutual information (MI), information entropy (EN) and standard deviation (STD). MI means the amount of information from both images. EN denotes the amount of information in the fused image. STD describes the edge performance in the fused image.

The experimental parameters of the PCNN were adopted as $q \times p = 3 \times 3$, $\alpha_L = 1.0$, $\alpha_\theta = 0.2$, $\beta = 3$, $V_L = 1.0$ and $V_\theta = 20$, and the linking weight W for a single neuron is expressed as

$$W = \begin{bmatrix} 0.707 & 1 & 0.707 \\ 1 & 0 & 1 \\ 0.707 & 1 & 0.707 \end{bmatrix}.$$

The number of maximum iterations was 200. The experimental results of the visual comparison are shown in Figures 5 and 6, and the experimental analysis of objective comparisons is listed in Table 1.

Figure 5 shows an image fusion performance comparison between the NSCT–PCNN-based algorithm and our proposed algorithms, which included two pairs of multifocus images, a1 and a2, and b1 and b2; two pairs of multisensor images, c1 and c2, and d1 and d2; and two pairs of SAR images, e1 and e2, and f1 and f2. In Figure 5(a1,a2), the bottom and top areas are clearer than those in the original images; however, the middle areas are not clear. That is because the middle areas of the two original images are unfocused. In Figure 5(b1,b2), there are two kinds of fused images in the right and left

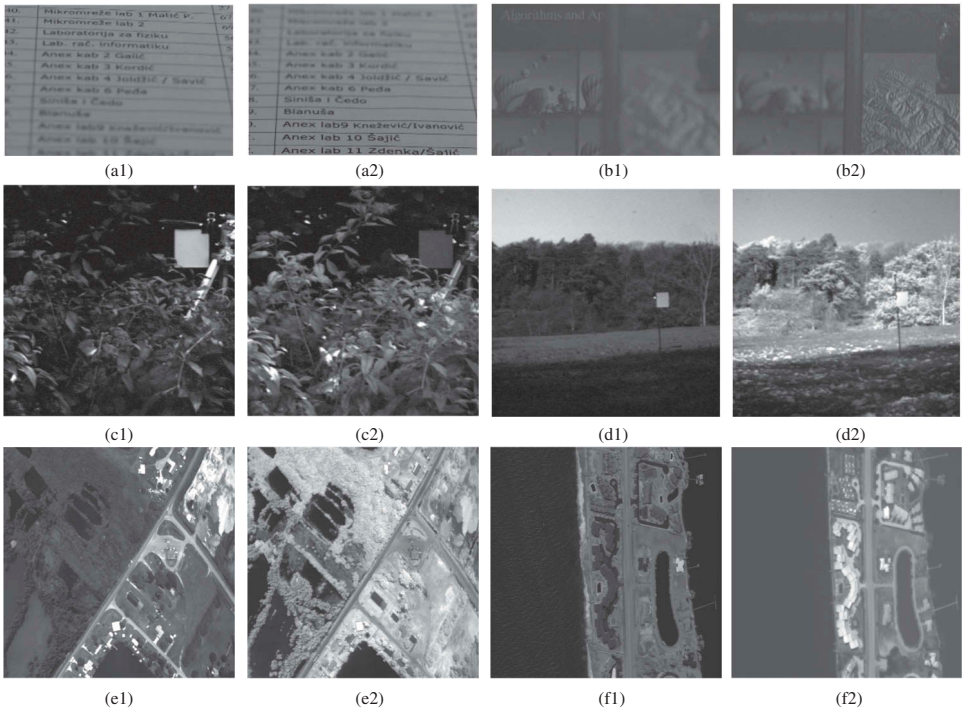

Figure 4. Original input images. (a1) Multifocus image 1.1, (a2) multifocus image 1.2, (b1) multifocus image 2.1, (b2) multifocus image 2.2, (c1) multisensor image 3.1, (c2) multisensor image 3.2, (d1) multisensor image 1.1, (d2) multisensor image 1.2, (e1) SAR image 1.1, (e2) SAR image 1.2, (f1) SAR image 2.1 and (f2) SAR image 2.2.

focuses, and we can see that the two image fusion algorithms can well be applied to multifocus images. Figure 5(c1,c2) and (d1,d2) are the two image fusion results of multisensor images. The testing results show that using the above two image fusion algorithms can make the image clearer than either of the two original images. Figure 5 (e1,e2) and (f1,f2) are two results of the image fusion of the SAR images that make the image clearer than either of the two original images. These results show that the proposed image fusion algorithm compares favourably with the state-of-the-art conventional NSCT–PCNN-based image fusion algorithm mentioned above. In this case, Figure 5(e1,e2) and (f1,f2) are all clear images; however, we found a difference in Figure 5(f1,f2) in fused image quality using the two algorithms. For this purpose, comparing Figure 6(a) with Figure 6(b), we can see that for the state-of-the-art conventional algorithm, there is a black area in the white square area that is different from the original image. Therefore, it can be concluded that the two filters are able to elicit a much greater response to the edges of the contrast image. On the other hand, we can also see that the proposed algorithm reduces the black area in the same region mentioned above. In that region, the fused image using the proposed fusion algorithm is much more natural than that fused by the state-of-the-art conventional hybrid NSCT and PCNN algorithm. That is because the proposed image fusion algorithm added two-filter processing to the low-frequency coefficients using Laplacian and average filters in

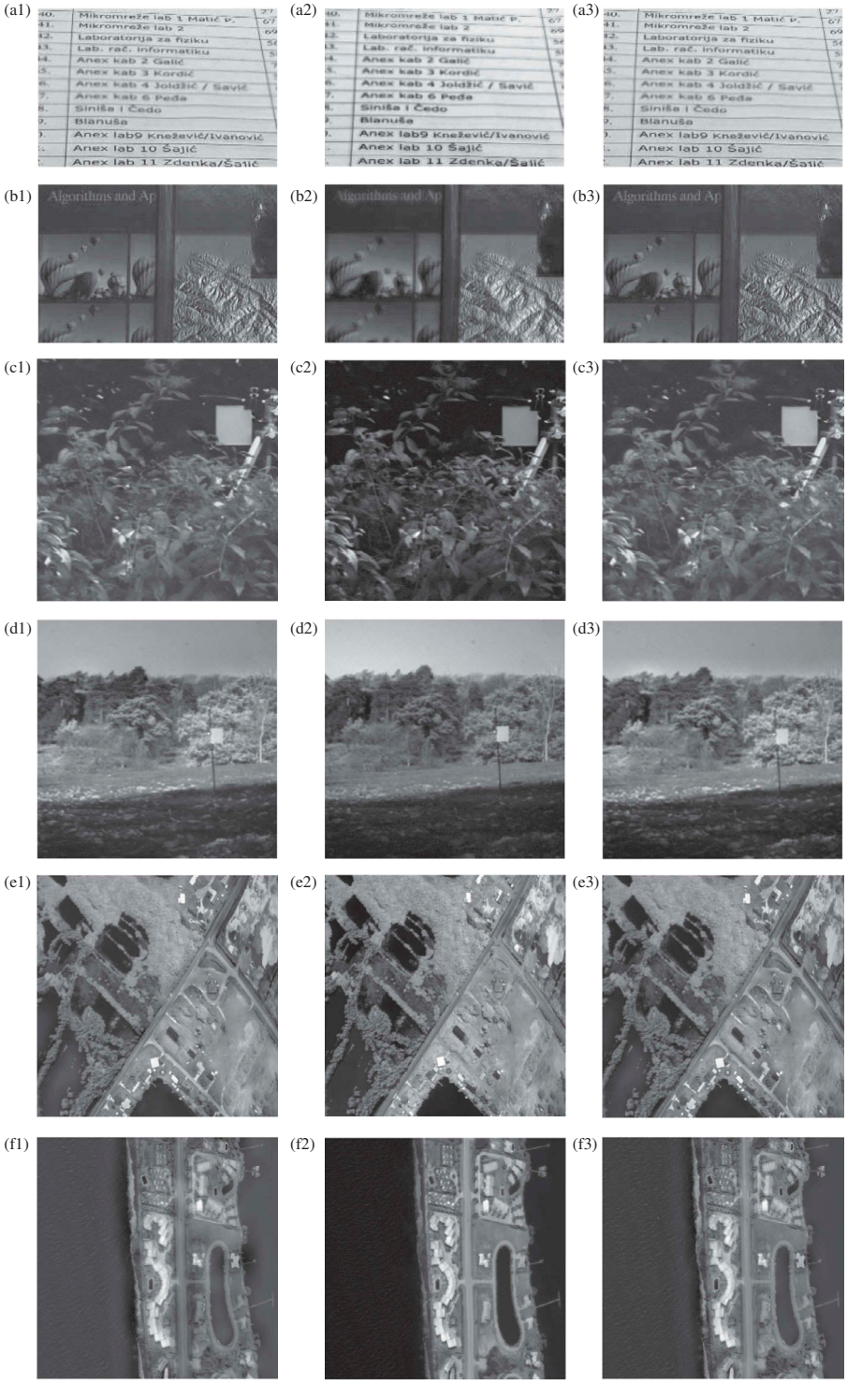

Figure 5. Images fused by different methods. (a1) NSCT with PCNN algorithm; (a2) PCA algorithm, (a3) proposed algorithm, (b1) NSCT with PCNN algorithm, (b2) PCA algorithm, (b3) proposed algorithm, (c1) NSCT with PCNN algorithm, (c2) PCA algorithm, (c3) proposed algorithm, (d1) NSCT with PCNN algorithm, (d2) PCA algorithm, (d3) proposed algorithm, (e1) NSCT with PCNN algorithm, (e2) PCA algorithm, (e3) proposed algorithm, (f1) NSCT with PCNN algorithm, (f2) PCA algorithm and (f3) proposed algorithm.

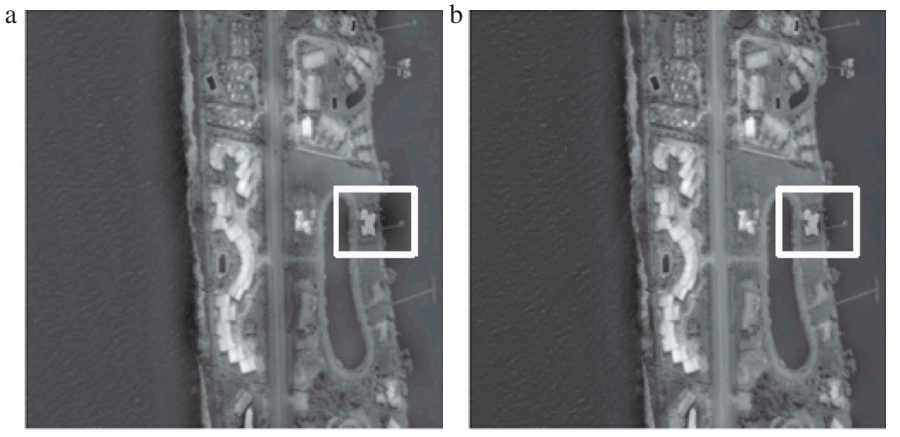

Figure 6. Difference between the fused images of two algorithms. (a) NSCT with PCNN algorithm and (b) proposed algorithm.

Table 1. Fusion performance comparison of different images between NSCT–PCNN, PCA and proposed algorithms.

Original image set	Fusion algorithm	Mutual information	Information entropy	Standard deviation
	NSCT–PCNN	3.3358	6.5846	34.335
Figure 4(a1,a2)	PCA	2.9981	5.4572	14.1412
	Proposed	3.4117	6.6395	34.782
	NSCT–PCNN	4.0951	6.6160	29.581
Figure 4(b1,b2)	PCA	4.0666	5.0644	9.7259
	Proposed	4.4141	6.6293	30.047
	NSCT–PCNN	3.4116	6.4332	32.192
Figure 4(c1,c2)	PCA	4.2708	6.3937	31.7225
	Proposed	3.7221	6.4690	32.718
	NSCT–PCNN	4.5043	7.3016	46.977
Figure 4(d1,d2)	PCA	5.6891	7.3916	55.7345
	Proposed	4.8209	7.4043	48.784
	NSCT–PCNN	2.8742	7.3450	43.588
Figure 4(e1,e2)	PCA	3.9304	7.3181	45.8893
	Proposed	3.0069	7.3640	44.097
	NSCT–PCNN	2.9908	6.5740	37.233
Figure 4(f1,f2)	PCA	4.5052	5.6732	30.8731
	Proposed	4.4141	6.6293	30.047

the frequency domain. The two filters above enhanced the characteristics and contrast performance of the important coefficients in the image decomposition, whereas the PCNN had no response to the insignificant coefficients when the modulation result of the neurons was less than the threshold value of the neuron ignition.

The performance comparison between the different fusion methods for the test images is shown in Figure 7.

Finally, we can show an objective evaluation of the test images in Table 1 between the NSCT–PCNN-based fusion algorithm and the proposed fusion algorithm, which also includes the PCA method. These experimental results show that the image fusion performance of the proposed algorithm is better overall than that of the state-of-the-art conventional hybrid NSCT–PCNN algorithm and the PCA method. Among the evaluation indices, the MI is better in

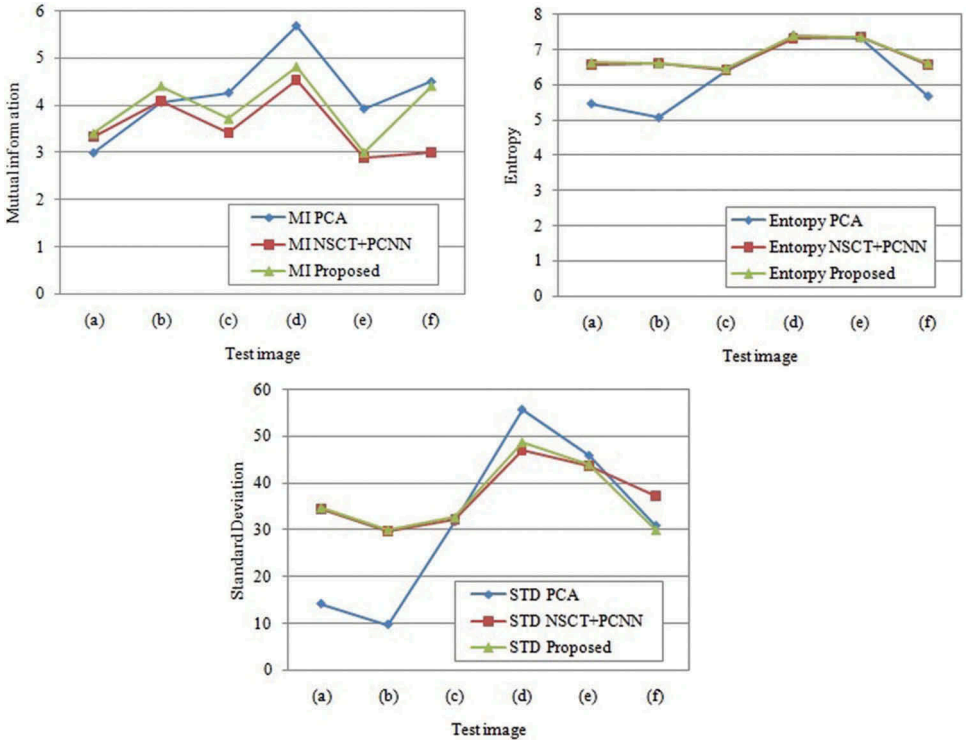

Figure 7. Performance comparison of different fusion methods for the test images. (a) Performance comparison for MI, (b) performance comparison for EN and (c) performance comparison for STD.

the proposed algorithm because it is higher 0.0759–0.3190 bit than the state-of-the-art conventional hybrid NSCT–PCNN algorithm and the PCA method; the EN is higher 0.0133–0.1027 bit; the STD is higher 0.447–1.807. These results show that the proposed algorithm allows the fused image to more easily obtain both images' information and is superior to the state-of-the-art conventional image fusion hybrid NSCT–PCNN algorithm and the PCA method.

5. Conclusion

This paper proposes a novel image fusion algorithm using NSCT and PCNN with digital filtering. We first processed the different levels of low-frequency subband coefficients that were decomposed in the frequency domain by using the NSCT. After that, the first two levels of low-frequency subband coefficients were duplicated and filtered by both Laplacian and average filters. The two filters enhanced the characteristics of the coefficients in the frequency domain because they corresponded to some pixels with the larger grey values in the spatial domain for an image decomposition. The obtained coefficients at various scales and directions in an image were then fused by the PCNN as the first-time fusion. In addition, the two kinds of decomposition coefficients, which were both low- and high frequency from the different images, were fused in a second fusion process. Finally, the fused image was reconstructed using the low- and high-

frequency subband coefficients at different-direction subbands in various scales by an inverse NSCT. The experimental results show that the performance of the image fusion algorithm proposed in this paper was better than that of the state-of-the-art conventional hybrid NSCT–PCNN algorithm and the PCA method.

Acknowledgement

We would like to say thanks to Duncan D.-Y. Po who is the author of the article entitled "Directional multiscale modeling of images using the contourlet transform" for valuable discussion.

Funding

This work was partly supported by the National Natural Science Foundation of China [Grant Numbers 61673314, 61573272 and 11504297] and MEXT/JSPS Grant-in-Aid for JSPS Fellows: [Grant Number 24·10018].

References

Chan, C.H., *et al*., 2013. Multiscale local phase quantization for robust component-based face recognition using kernel fusion of multiple descriptors. *IEEE Transactions on Pattern Analysis and Machine Intelligence*, 35 (5), 1164–1177. doi:10.1109/TPAMI.2012.199

Da Cunha, A.L., Zhou, J., and Do, M.N., 2006. The nonsubsampled contourlet transform: theory, design, and applications. *IEEE Transactions on Image Processing*, 15 (10), 3089–3101. doi:10.1109/TIP.2006.877507

Eckhorn, R., *et al*., 1990. Feature linking via synchronization among distributed assemblies: simulations of results from cat visual cortex. *Neural Computation*, 2, 293–307. doi:10.1162/neco.1990.2.3.293

Ge, Y. and Li, X., 2010. Image fusion algorithm based on pulse coupled neural networks and nonsubsampled contourlet transform. *In*: *Proceedings of second international workshop on education technology and computer science*, Wuhan, March 6-7, 27–30. Los Alamitos, CA: IEEE Computer Society.

Jang, J.H., Bae, Y., and Ra, J.B., 2012. Contrast-enhanced fusion of multisensor images using subband-decomposed multiscale retinex. *IEEE Transactions on Image Processing*, 21 (8), 3479–3490. doi:10.1109/TIP.2012.2197014

Johnson, J.L. and Padgett, M.L., 1999. PCNN models and applications. *IEEE Transactions on Neural Networks*, 10 (3), 480–498. doi:10.1109/72.761706

Li, S.T. and Yang, B., 2010. Hybrid multiresolution method for multisensor multimodal image fusion. *IEEE Sensors Journal*, 10 (9), 1519–1526. doi:10.1109/JSEN.2010.2041924

Lindblad, T. and Kinser, J.M., 2005. *Image processing using pulse-coupled neural networks*. Berlin Heidelberg: Springer-Verlag.

Fu, L., Jin, L., Huang, C., 2012. Image fusion algorithm based on simplified PCNN in nonsubsampled contourlet transform domain. *Procedia Engineering*, 29, 1434–1438. doi:10.1016/j.proeng.2012.01.151

Núñez, J., *et al*., 1999. Multiresolution-based image fusion with additive wavelet decomposition. *IEEE Transactions on Geoscience and Remote Sensing*, 37 (3), 1204–1211. doi:10.1109/36.763274

Petrovic, V.S. and Xydeas, C.S., 2004. Gradient-based multiresolution image fusion. *IEEE Transactions on Image Processing*, 13 (2), 228–237. doi:10.1109/TIP.2004.823821

Qu, X., *et al*., 2008. Image fusion algorithm based on spatial frequency-motivated pulse coupled neural networks in nonsubsampled contourlet transform domain. *Acta Automatica Sinica*, 34 (12), 1508–1514. doi:10.1016/S1874-1029(08)60174-3

Stokman, H. and Gevers, T., 2007. Selection and fusion of color models for image feature detection. *IEEE Transactions on Pattern Analysis and Machine Intelligence*, 29 (3), 371–381. doi:10.1109/TPAMI.2007.58

Wang, H., *et al*., 2013a. Multi-atlas segmentation with joint label fusion. *IEEE Transactions on Pattern Analysis and Machine Intelligence*, 35 (3), 611–623. doi:10.1109/TPAMI.2012.143

Wang, L., *et al*., 2016. An automatic segmentation and classification framework based on PCNN model for single tooth in microCT images. *PLoS One*, 11 (6). doi:10.1371/journal.pone.0157694

Wang, X., *et al*., 2013b. Image denoising using SVM classification in nonsubsampled contourlet transform domain. *Information Sciences*, 246, 155–176. doi:10.1016/j.ins.2013.05.028

Wang, Z., Ma, Y., and Gu, J., 2010. Multi-focus image fusion using PCNN. *Pattern Recognition*, 43, 2003–2016. doi:10.1016/j.patcog.2010.01.011

Xie, X., Lai, J., and Zheng, W., 2010. Extraction of illumination invariant facial features from a single image using nonsubsampled contourlet transform. *Pattern Recognition*, 43, 4177–4189. doi:10.1016/j.patcog.2010.06.019

Yang, B. and Li, S., 2010. Multifocus image fusion and restoration with sparse representation. *IEEE Transactions on Instrumentation and Measurement*, 59 (4), 884–892. doi:10.1109/TIM.2009.2026612

Yang, G., *et al*., 2010. A novel design approach for contourlet filter banks. *IEICE Transactions on Information and Systems*, E93-D (7), 2009–2011. doi:10.1587/transinf.E93.D.2009

Yang, L., Guo, B.L., and Ni, W., 2008. Multimodality medical image fusion based on multiscale geometric analysis of contourlet transform. *Neurocomputing*, 72, 203–211. doi:10.1016/j.neucom.2008.02.025

Yang, S., *et al*., 2009. Fusion of multiparametric SAR images based on SW-nonsubsampled contourlet and PCNN. *Signal Processing*, 89 (12), 2596–2608. doi:10.1016/j.sigpro.2009.04.027

Zhang, Q. and Guo, B., 2009. Multifocus image fusion using the nonsubsampled contourlet transform. *Signal Processing*, 89, 1334–1346. doi:10.1016/j.sigpro.2009.01.012

Zheng, S., *et al*., 2007. Multisource image fusion method using support value transform. *IEEE Transactions on Image Processing*, 16 (7), 1831–1839. doi:10.1109/TIP.2007.896687

Zhou, J., Da Cunha, A.L., and Do, M.N., 2005. Nonsubsampled contourlet transform: construction and application in enhancemen. In: *Proceedings of international conference on image processing (ICIP)*, September *11-14*. Genoa: IEEE, 469–472.